Dalton Transactions

ROYAL SOCIETY OF CHEMISTRY

PAPER

View Article Online
View Journal | View Issue

Check for updates

Cite this: *Dalton Trans.*, 2024, **53**, 8243

A detailed density functional theory exploration of the photodissociation mechanism of ruthenium complexes for photoactivated chemotherapy†

Daniele Belletto, Fortuna Ponte,* Gloria Mazzone and Emilia Sicilia *

Received 20th March 2024,
Accepted 15th April 2024

DOI: 10.1039/d4dt00834k

rsc.li/dalton

Polypyridyl Ru(II) complexes have attracted much attention due to their potential as light-activatable anti-cancer agents in photoactivated chemotherapy (PACT). The action of ruthenium-based PACT compounds relies on the breaking of a coordination bond between the metal center and an organic ligand *via* a photosubstitution reaction. Here, a detailed computational investigation of the photophysical properties of a novel trisheteroleptic ruthenium complex, $[Ru(dpp)(bpy)(mtmp)]^{2+}$ (dpp = 4,7-diphenyl-1,10-phenanthroline, bpy = 2,2′-bipyridine and mtmp = 2-methylthiomethylpyridine), has been carried out by means of DFT and its time-dependent extension. All the aspects of the mechanism by which, upon light irradiation, the mtmp protecting group is released and the corresponding aquated complex, able to bind to DNA inducing cell death, is formed have been explored in detail. All the involved singlet and triplet states have been fully described, providing the calculation of the corresponding energy barriers. The involvement of solvent molecules in photosubstitution and the role played by pyridyl–thioether chelates as caging groups have been elucidated.

Open Access Article. Published on 17 April 2024. Downloaded on 2/20/2026 5:59:16 PM.
This article is licensed under a Creative Commons Attribution-NonCommercial 3.0 Unported Licence.

Introduction

Precise spatial and temporal control of the activity of externally applied chemical agents in their interaction with complex biological systems for therapeutic purposes is of special significance aiming at achieving a greater action specificity. Even though a large number of drugs able to be activated by specific stimuli, such as redox, pH, enzyme and temperature, have been proposed,[1] differences in the cellular environment are very narrow and extremely sensitive compounds are required. Intense focused light sources accessible today, instead, make photoactivation a very attractive alternative and therapies relying on the use of chemotherapeutic compounds that respond to light of appropriate wavelength are currently the object of a great deal of attention. The term "photoactivated chemotherapy" (PACT) was proposed by Sadler *et al.* in 2009[2,3] and has been used since then to identify therapeutic strategies in oncology based on the use of biologically active metal complexes acting as prodrugs able to exert their cytotoxic action when irradiated. This kind of approach should overcome drawbacks such as dose escalation, drug resistance, and severe side effects of the drugs that are currently in use, which lack specificity and have low bioavailability.[4,5] Three main modes of activation for inorganic compounds used in PACT are usually taken into consideration: (i) photoreduction in the cellular reducing environment to produce the corresponding reduced active complexes together with the released ligands; (ii) photosubstitution leading to a ligand replaced by a solvent molecule, typically water; (iii) photorelease of small biological effector molecules inactivated by coordination to a metal centre.

PACT is often compared to photodynamic therapy (PDT) since both therapies rely on the use of light for activating drugs that are relatively non-toxic in the dark. Nevertheless, these two classes of treatments present many differences.[6] PDT agents are photostable, whereas PACT agents change their chemical formula upon irradiation, and it is worth noting that the major advantage of PACT over PDT is the oxygen-independent mechanism of action of the drugs that enhances their efficiency in hypoxic environments such as those of tumours.

Transition metal containing complexes, owing to their rich photophysics and photochemistry that can also be tuned properly by varying the metal centre and/or ligands, are considered very promising compounds to be used in PACT given their capacity to modify their structure upon light irradiation. The ideal candidate should be a prodrug stable and nontoxic to cells in the dark, but activatable within tumour tissues by light of relatively long wavelengths, and able to both penetrate in depth and minimize photodamage of endogenous com-

Department of Chemistry and Chemical Technologies, Università della Calabria, Ponte P. Bucci, 87036 Arcavacata di Rende, CS, Italy. E-mail: emilia.sicilia@unical.it, fortuna.ponte@unical.it

†Electronic supplementary information (ESI) available: Optimized geometry of the **Ru** complex, TDDFT benchmark, singlet and triplet transitions, NTOs, selected bond lengths of Ta, Tb, Tc and Td triplet states, and relaxed potential energy scans. See DOI: **https://doi.org/10.1039/d4dt00834k**

Open Access Article. Published on 17 April 2024. Downloaded on 2/20/2026 5:59:16 PM.
This article is licensed under a Creative Commons Attribution-NonCommercial 3.0 Unported Licence.

pounds. Metal complexes including Pt(IV),[7] Re(I),[8] and Ir(III)[9] together with Rh(III)[10] and Ru(II)[11,12] have all been investigated extensively for this purpose. Photoactivatable Ru(II)-centred complexes, in particular polypyridyl ruthenium compounds, emerged as promising candidates owing to their low ligand exchange propensity observed in the dark, together with their high photoreactivity. Various studies have reported that they may undergo photosubstitution reactions, mediated by solvent molecules, forming photoproducts having significantly higher cytotoxicity compared to the precursor complex.[13–16] These resultant "uncaged" metal Ru(II) complexes can bind DNA in a manner similar to cisplatin, thus inducing cell death.[17]

Bonnet and co-workers have recently presented a new ruthenium complex, $[Ru(dpp)(bpy)(mtmp)]^{2+}$ (Scheme 1), bearing three different bidentate chelating ligands: dpp (4,7-diphenyl-1,10-phenanthroline) and bpy (2,2′-bipyridine), which are non-photocleavable spectator groups, and an mtmp ligand (2-methylthiomethylpyridine).[18] This complex will be called **Ru** complex from now on. The advantage of using thioether ligands is that their softness allows efficient coordination to Ru(II) in the ground state, while their photosubstitution efficiency is greater than that of pyridines as a consequence of the relative weakness of the Ru–S bond compared to the Ru–N one in the excited state.[19] The mtmp ligand, indeed, acts as a photolabile group, which is photosubstituted by solvent molecules under green light irradiation generating the active DNA photobinding agent.[18]

Stimulated by the experimentally reported efficacy of such a novel synthesized PACT agent, a detailed computational investigation of the photophysical properties of the complex has been carried out by means of density functional theory (DFT). Over the course of years, new information has been added through the use of computational tools to the description of the mechanism of photosubstitution for the detachment of both mono- and bi-dentate ligands and to the rationalization of the observed behaviours in terms of the involved triplet excited states.[20–24] Here, the outcomes of our computational analysis are reported aiming at helping the comprehension of the described phenomena and the synthesis of new efficacious PACT agents. All the mechanistic aspects of the photodissociation process have been explored in detail and all the involved singlet and triplet states have been fully described with the aim to contribute to addressing two of the unresolved issues that need clarification in order to ultimately design efficacious **Ru** complexes suitable for PACT application. One aim is general and concerns the involvement of solvent molecules in photosubstitution and the other is specific about the excellent role played by pyridyl–thioether chelates as caging groups.

Results and discussion

The fully optimized ground state (GS) structure of the **Ru** complex, in water solvent and without imposing any symmetry constraint, is shown in Fig. S1 of the ESI† along with the main structural parameters. The trisheteroleptic complex adopts a distorted octahedral geometry. The average Ru–N(bpy) and Ru–N(dpp) bond lengths are 2.102 and 2.120 Å, respectively, whereas the Ru–N(mtmp) bond length is 2.150 Å. The Ru–S bond distance is significantly longer by about 0.25 Å. The bpy and dpp bite angles are 77.8 degrees, while that of the mtmp ligand is 81.1 degrees.

Photophysical properties of the Ru complex

In order to properly describe the photophysical processes accounting for PACT action, a preliminary benchmarking of the exchange and correlation functionals has been carried out. A superposition of the **Ru** complex simulated spectra and the experimental one and a comparison of the calculated maximum absorption wavelengths with those experimentally available, obtained in acetonitrile solvent, are provided in Fig. S2 and Table S1 of the ESI,† respectively. From the reported data, the M05 functional emerges as the functional that better simulates the experimental feature and it has been employed, hence, for its complete characterization: both the examination of the photochemical characteristics and the light-induced reaction mechanisms.

The UV-vis spectrum of the **Ru** complex has been thus recorded in the solvent that could better mimic the physiological environment, that is water, and is reported in Fig. 1, where the most important transitions are included.

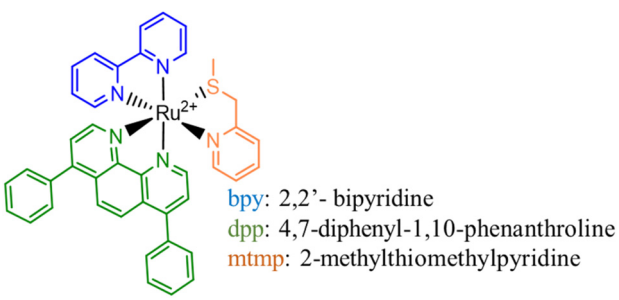

Scheme 1 Schematic representation of the structure of the Ru(II) complex under investigation.

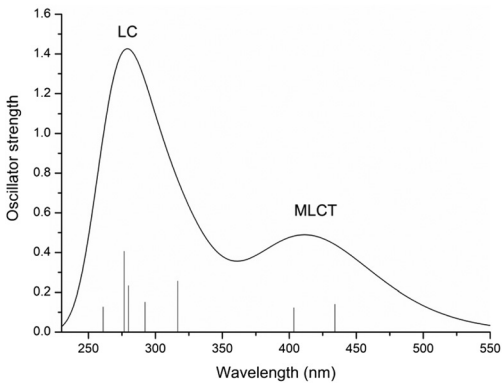

Fig. 1 Calculated UV-vis absorption spectrum of the **Ru** complex in water at the M05/6-31G** (SDD for Ru) level of theory.

This journal is © The Royal Society of Chemistry 2024

Open Access Article. Published on 17 April 2024. Downloaded on 2/20/2026 5:59:16 PM.
This article is licensed under a Creative Commons Attribution-NonCommercial 3.0 Unported Licence.

The main data describing the absorption spectrum of **Ru** are collected in Table S2 of the ESI.† Only the electronic transitions with an oscillator strength (f) higher than 0.01, considered to be essential for determining the different absorption bands, are reported. The only exception is the reported first transition, for the S1 state. The composition percentage of molecular orbitals, for each of the listed transitions, is also included. Natural Transition Orbital (NTO) plots[25] for the most important transitions of the spectrum are shown in Fig. S3.† For the **Ru** complex, the calculated absorption spectrum displays essentially two bands. A first weaker absorption band, of appreciable intensity, is observed in the range of 350–500 nm and centred at 434 nm, a value that reproduces very well the maximum absorption wavelength of 430 nm experimentally detected.[15] TDDFT calculations assign this transition to the S5 singlet excited state and the analysis carried out with the TheoDORE (theoretical density, orbital relaxation and exciton analysis) package[26] confirms a band with the MLCT character. Indeed, all the electronic transitions originating from such a band involve a charge transfer from a molecular orbital primarily located on the metal (*i.e.* HOMO (H) and H-2) to an orbital outspread on one of the two N^N ligands, either bpy or dpp. In particular, the excitation to the S1 state, calculated at 486 nm (Tr1), originates from the mixed transitions H → L + 1 (61%) and H → L (33%) that mainly involve the bpy ligand. The most intense peak at higher energy, between 250 and 350 nm, is found at 275 nm. Despite a little contribution of the type MLCT, the band is characterized by electronic transitions that are mainly centred on the ligand, as confirmed by the NTOs and TheoDORE analysis.

Excited states study

Considering that the lifetime of singlet excited states is approximately five times shorter than that of triplet states (10^{-8} *vs.* 10^{-3} s), it seems reasonable to suggest that the pathway for converting the system under investigation into a diaquo species may entail an excited triplet state instead of a singlet one. Specifically, for Ru-based PACT agents, it is generally accepted that photoactivated dissociation and solvolysis occur due to the population of a dissociative triplet metal-centred ^{3}MC state from a triplet metal–ligand charge transfer ^{3}MLCT state that lies close enough in energy. Such an ^{3}MLCT state, in turn, is generated by a metal-to-ligand charge-transfer singlet excited state (^{1}MLCT) that efficiently spin–flips to a triplet one.[27–30] ^{1}MLCT to ^{3}MLCT transitions are usually very fast and thermally non-activated, whereas ^{3}MLCT to ^{3}MC conversions can entail the overcoming of an activation barrier and take time. With Kasha's rules in mind,[31] it seems reasonable to hypothesize that when the S5 state, identified as the bright state, is populated by photon absorption, an internal conversion can occur before the intersystem crossing (ISC) process with consequent population of the first singlet excited state S1. From here a spin–flip is required to achieve the PACT active state, a triplet state. In order to properly identify and characterize the triplet states responsible for the photodissociation process and then describe the photoactivity of **Ru**, a primary investigation, within the vertical approximation, of the photophysical features of the triplet states below the S1 and T1–T6 has been performed. The energies and the characteristics of the selected six triplet states are reported in Table S3 of the ESI,† whereas the NTO plots for these triplet excited states are shown in Fig. S4.† While the first four triplet states share the mixed characteristics of LC/MLCT, the last two exhibit a certain contribution of the MC characteristic together with the CT from the metal to the ligand. To establish the feasibility of ISC processes from S1 to the triplet manifold, the spin–orbit matrix elements and the energy difference between the singlet and triplet states lying below have been calculated and are reported in Table 1. Looking at these data, it is worth noting that the triplet states show a common behaviour, independent of their characteristics, and that the influence of the metal is evident from the values of the SOC elements computed for all the S1 → Tn (n = 1–6) radiationless transitions. Therefore, based on the high SOC values, it is plausible to suggest that the transition to the lowest singlet excited state (S1) is followed by an efficient ISC to the triplet manifold.

Once the feasibility of ISC processes is established, the structures of the involved singlet and triplet excited states have been optimized within the TDDFT approximation in order to properly characterize the triplet states and compute the effective energy splitting between the coupled states. The structures obtained for the triplet states have been subsequently used as starting points for the optimization within the unrestricted Kohn–Sham formalism (UKS),[34,35] as it is reported to help in reducing the instability of excited triplet states involving charge transfer. The analysed triplet excited states converged into four distinct states denoted as Ta, Tb, Tc and Td. Their optimized structures, together with the corresponding spin density distributions, were used to determine their characteristics and are reported in Fig. 2, where the spin density values on the Ru atom and the relative energies calculated with respect to the ground state GS are also included. Furthermore, a comparison of the main bond distances of the calculated triplet states with those of the GS is reported in Table S4.† Cartesian coordinates of GS and Ta, Tb, Tc and Td triplet states are collected in Table S5.† As it clearly appears, in all the intercepted triplet structures, the bonds with the mtmp group are lengthened, supporting the dissociative characteristic of these triplets leading to the detachment of

Table 1 Spin–orbit coupling constants (SOC, cm^{-1}) between the excited singlet S1 and triplet states T1–T6 together with their energy difference (ΔE, eV)

Tn	SOC[a] (cm^{-1})	ΔE (eV)
T1	65	0.56
T2	239	0.33
T3	133	0.26
T4	201	0.08
T5	322	0.06
T6	289	0.01

[a] Calculated as in ref. 32 and 33.

Open Access Article. Published on 17 April 2024. Downloaded on 2/20/2026 5:59:16 PM.
This article is licensed under a Creative Commons Attribution-NonCommercial 3.0 Unported Licence.

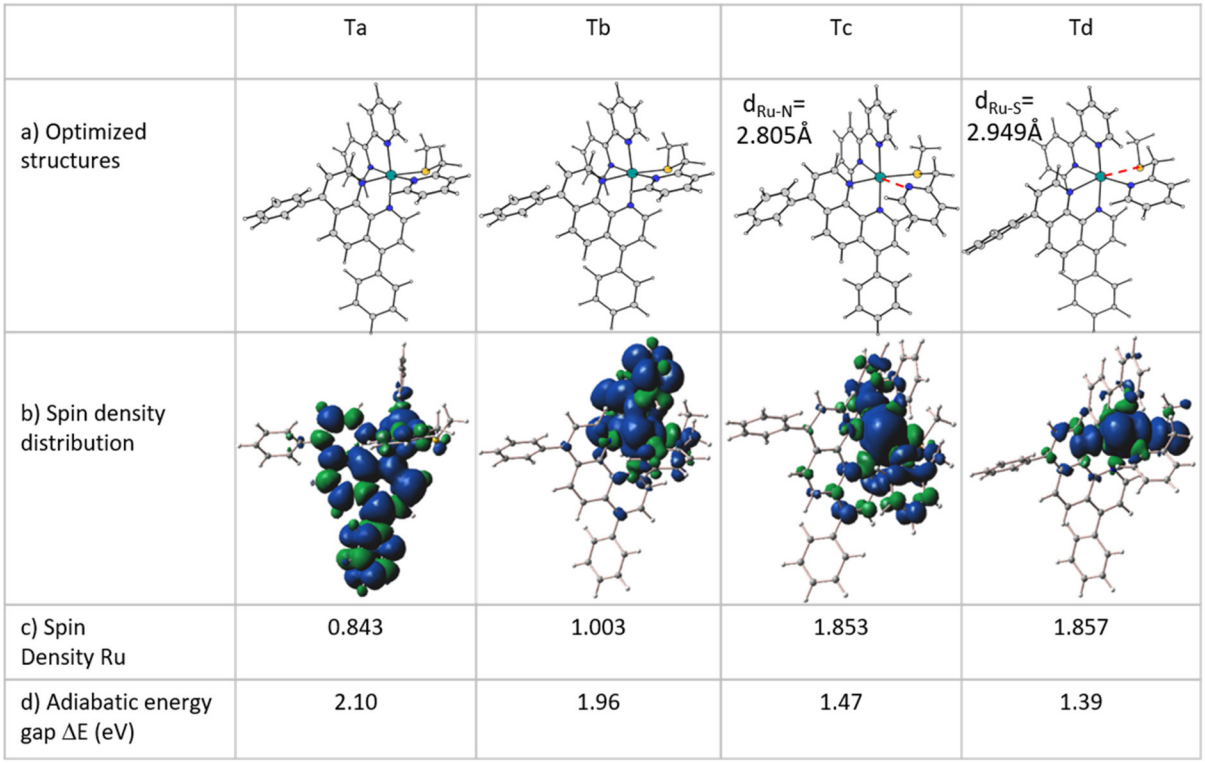

Fig. 2 (a) Structure of optimized triplet states Ta, Tb, Tc and Td within the unrestricted DFT formalism. (b) Computed spin density distributions of the intercepted triplet states. (c) Spin density values (SD in a.u.) on the ruthenium metal center. (d) Energy gap between the optimized triplet states and the S0 ground state.

the S,N-donor ligand. In particular, the structures of the triplet states Ta and Tb show modest differences compared to that of the ground state (see Table S4†), while the optimized triplet excited states Tc and Td have been found to be dissociative with respect to the mtmp ligand and are responsible for the photoreactivity of this complex.

Tc and Td triplet states appear to be characterized by a significant reorganization in the coordination sphere of the Ru centre. In Tc, the detachment of the pyridyl arm of the mtmp ligand takes place with an increase in the Ru–N bond distance of about 0.7 Å and a deviation of 67.9 degrees with respect to the plane containing the metal. This rearrangement is accompanied also by an increase in the length of the Ru–N bond in the *trans* position by about 0.3 Å. The lowest energy triplet state Td is characterized, instead, by a clear elongation of the Ru–S bond and shows a large deviation from the GS structure with a strong distortion of the metal coordination sphere. The Ru–S distance increases by approximately 0.6 Å and the pendant arm containing the sulphur donor atom lies at 51.1 degrees with respect to the plane containing the metal centre, while the *trans* Ru–N bond lengthens by more than 0.3 Å. All the obtained triplet states have been properly characterized and all the possible photophysical processes examined. Looking at Fig. 2b, the spin density distribution plot confirms the MLCT characteristic of the Ta and Tb triplets.

The Mulliken spin density near unity on the Ru(II) centre is indicative of one unpaired electron on the metal centre in the excited state as it should be expected for the ^{3}MLCT state. In contrast, the spin density values of about 1.9 a.u. for both Tc and Td triplet states show that the unpaired electrons are essentially localized at the Ru centre as for a triplet with ^{3}MC nature. This nature of both Tc and Td states facilitates ligand photodissociation. The relative energies of the photoactivated excited states follow the order S1 (^{1}MLCT) > Ta (^{3}MLCT) > Tb (^{3}MLCT) > Tc (^{3}MC) > Td (^{3}MC). The **Ru** complex shows more stable metal-centred excited states, ^{3}MC states, than the ^{3}MLCT triplet state, a characteristic that enhances the probability of an internal conversion (^{3}MLCT → ^{3}MC state). Relaxed scans have been performed on the triplet potential energy surfaces to determine the barriers for the conversion from the Tb state to the Tc and Td ones. The corresponding relaxed potential energy surfaces are shown in Fig. 3 as obtained by varying the S1–C2–C3–N4 and N4–C3–C2–S1 dihedral angles by −2.0 degrees for Tc and Td states, respectively. In both cases, an abrupt transition from the ^{3}MLCT state to the ^{3}MC one is observed for an estimated barrier of 7.0 kcal mol^{-1} along the path for the Tc state formation and of 4.5 kcal mol^{-1} along the path for the Td state generation. This behaviour indicates that the electron density transition does not occur smoothly. Therefore, we can assume that when the dihedral angles change and the complex geometry is distorted, the involved orbitals don't mix.[36]

The simplified Jablonski diagram that represents the key photophysical processes in the **Ru** complex is reported in

 This journal is © The Royal Society of Chemistry 2024

Open Access Article. Published on 17 April 2024. Downloaded on 2/20/2026 5:59:16 PM.
This article is licensed under a Creative Commons Attribution-NonCommercial 3.0 Unported Licence.

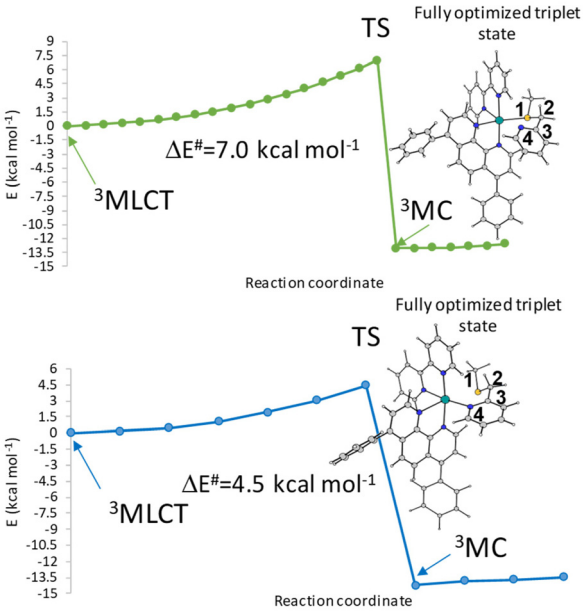

Fig. 3 Relaxed potential energy scans from the ^{3}MLCT state to ^{3}MC (a) Tc and (b) Td of the **Ru** complex calculated by varying the S1–C2–C3–N4 and N4–C3–C2–S1 dihedral angles (°).

Fig. 4. Looking at the energy gaps S1–T*n*, the triplet state Ta (^{3}MLCT) that lies at an energy close to the S1 state (^{1}MLCT) could be populated through an ISC mechanism. The intersystem crossing process can be followed by a fast internal conversion and the triplet Tb can be populated. The state Tb (^{3}MLCT) can either return to the ground state by radiative deactivation or it can evolve into a nonradiative triplet metal-centred state (^{3}MC) Tc or Td, lying below the Tb (^{3}MLCT) state, leading to ligand dissociation.

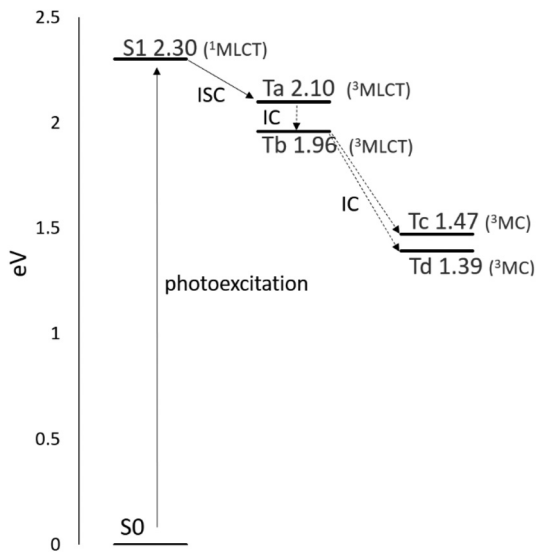

Fig. 4 Simplified Jablonski diagram depicting the key photophysical processes for the **Ru** complex: photoexcitation, intersystem crossing (ISC), and internal conversion (IC). The diagram highlights that ^{3}MC states fall below the ^{3}MLCT states.

A strategy commonly used to enhance the photosubstitution efficiency that decreases the ^{3}MLCT-^{3}MC energy gap or even inverts their energy order to favor the population of the ^{3}MC states consists of introducing steric strain on the dissociating ligand.[37–39] Alternatively, electronic effects can elicit photosubstitution, as assumed in the present case, and for some ligands, this effect is due to the ^{3}MLCT state destabilization.[40] Since for pyridyl–thioether chelates no indication has been given about their influence on photosubstitution, the analysis of the molecular orbitals for the **Ru** complex has been compared with that of other three complexes, which are $[Ru(bpy)_3]^{2+}$, $[Ru(phen)(bpy)_2]^{2+}$ with phen = 1,10-phenanthroline, and $[Ru(mtmp)(bpy)_2]^{2+}$ (Fig. 5). The three highest occupied molecular orbitals (HOMOs) are, as expected, metallic t_{2g} orbitals (d_{xy}, d_{xz}, d_{yz}) and are separated from the lowest unoccupied molecular orbital (LUMO) by an energy gap of 3.82 eV. The LUMOs are composed mainly of ligand centered π* orbitals. Specifically, the π* orbitals of the bpy and dpp ligands are involved. Higher in energy lie the metal-centered (e_g*) vacant MOs (dσ*) showing σ-antibonding interactions between the $d_{x^2-y^2}$ and d_{z^2} orbitals of the metal and the S and N atoms of the mtmp ligand. On going from the reference $[Ru(bpy)_3]^{2+}$ to $[Ru(phen)(bpy)_2]^{2+}$, it is possible to deduce that the presence of the phen ligand does not introduce any significant change, except for a further degeneration removal of the HOMO d orbitals. The comparison between $[Ru(phen)(bpy)_2]^{2+}$ and $[Ru(mtmp)(bpy)_2]^{2+}$, instead, shows clearly that substitution of the bpy ligand with mtmp causes a slight increase of the HOMO–LUMO energy gap due to slight stabilization of the HOMO and, very importantly, stabilization of the vacant MOs (dσ*) that are primarily $d_{x^2-y^2}$ and d_{z^2}-like orbitals responsible for the generation of the ^{3}MC states. A very similar diagram is obtained when the **Ru** MOs are examined involving stabilization of the ^{3}MC states, which accelerates the photosubstitution reaction.

Mechanism of Ru complex photodissociation

When exposed to visible light, ruthenium complexes undergo photochemical substitution reactions, where one of the ligands in the coordination sphere of the metal centre is replaced by solvent molecules. Over the years, the intricate nature of these systems has limited the exploration of their photoactivation mechanism. Particularly, from a theoretical perspective, the investigation of excited triplet states involves their challenging optimization.

Here, we report the detailed computational analysis of all the steps of the photoactivation mechanism of a ruthenium complex, including those leading to the formation of the final active solvated complexes, simulated with water molecules used to mimic the physiological environment. It is worth underlining that the triplet pathway has been built up starting from the optimized structures of the triplet states lying below the bright state and the transition states located and checked for their connection with the appropriate minima. Explicit

Open Access Article. Published on 17 April 2024. Downloaded on 2/20/2026 5:59:16 PM.
This article is licensed under a Creative Commons Attribution-NonCommercial 3.0 Unported Licence.

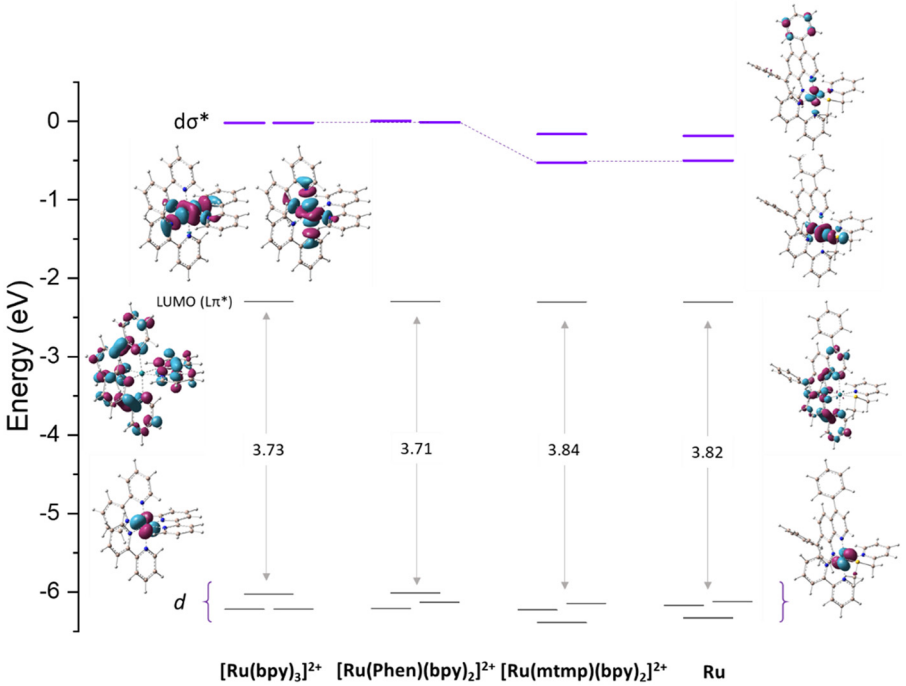

Fig. 5 Energy diagram of the molecular orbitals of the **Ru** complex compared with those of $[Ru(bpy)_3]^{2+}$, $[Ru(phen)(bpy)_2]^{2+}$ (phen = phenanthroline), and $[Ru(mtmp)(bpy)_2]^{2+}$ with representative plots of HOMOs, LUMOs and dσ* orbitals.

water molecules have been included in the model and the transition states for their coordination have been intercepted. Based on all the data described above and the experimental results,[18] two viable pathways for the activation by light of the **Ru** complex, shown in Scheme 2, can be proposed involving the previously described ^{3}MLCT (Ta, Tb) and ^{3}MC (Tc, Td) states.

Scheme 2 describes the whole process by which the biaquated photoproducts, the real cytotoxic species, are generated through photoinduced ligand dissociation. The excitation, taking place when the **Ru** complex is exposed to light of appropriate wavelength, leads to the population of the ^{1}MLCT state (^{1}Ru*), followed by an efficient ISC process that allows the formation of the excited ^{3}MLCT state Ta which could contribute to populate the Tb state by internal conversion, which represents a key intermediate in the complex photoactivation reaction. The second step consists of ligand dissociation. The triplet Tb can be deactivated by the population of the nearby ^{3}MC states with dissociative characteristics.

As stated above, two distinct ^{3}MC states, named Tc and Td, have been identified for the **Ru** complex. It is interesting to note that in both ^{3}MC states, one of the arms of the mtmp

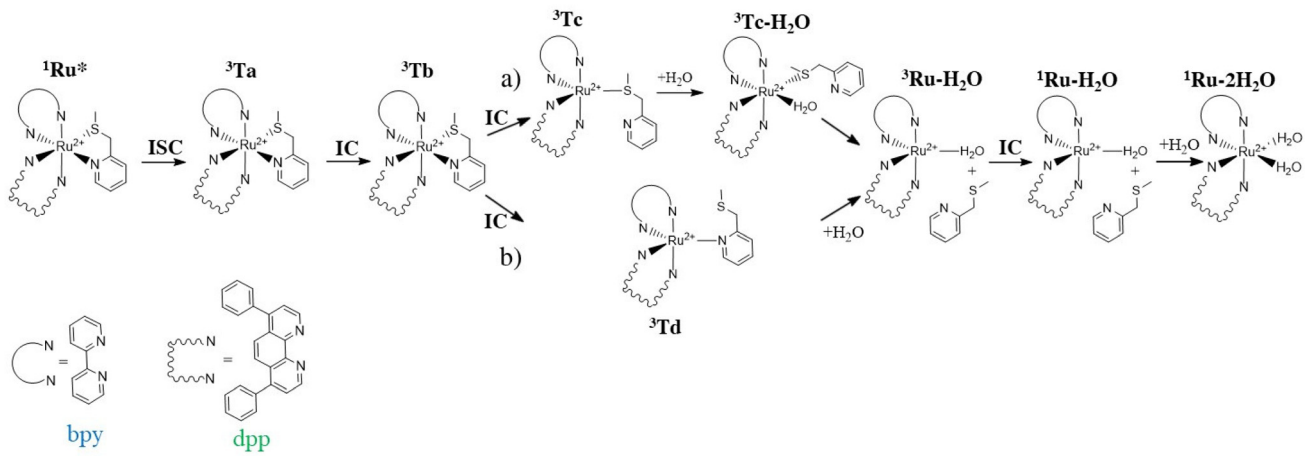

Scheme 2 Proposed activation pathways of the **Ru** complex involving both ^{3}MC (a) Tc and (b) Td states as intermediates for the formation of biaquated photoproducts having cytotoxic activity.

 This journal is © The Royal Society of Chemistry 2024

Open Access Article. Published on 17 April 2024. Downloaded on 2/20/2026 5:59:16 PM.
This article is licensed under a Creative Commons Attribution-NonCommercial 3.0 Unported Licence.

ligand is almost detached, resulting in the formation of an intermediate to be considered five-coordinated. From here, the reaction path bifurcates for the formation of a monoaquated complex that occurs in the next step. Along the pathway named (a), after the formation of the intermediate triplet Tc, the reaction proceeds with a stepwise ligand substitution. In the first step, a water molecule enters the coordination sphere of the metal, thereby restoring hexa-coordination to the ruthenium atom (^{3}Tc–H_2O). In the subsequent second step, the ruthenium mono-aquated complex named ^{3}Ru–H_2O is generated with the definitive detachment of the mtmp ligand. Along the triplet pathway named (b), from the intermediate triplet Td state, the formation of the mono-aquated ruthenium complex ^{3}Ru–H_2O occurs in one step through an associative ligand substitution of the mtmp ligand by a water molecule. Both triplet states, Tc and Td, produce the same intermediate, ^{3}Ru–H_2O. The last step of the process, that is the formation of the biaquated complex, takes place along a ground state singlet path. Indeed, after the formation of the mono-aquated species, the coordination complex may return to its ground state (^{1}Ru–H_2O) and the coordination of the second water molecule can occur forming the final photoproduct ^{1}Ru–$2H_2O$, the desired cytotoxic species. The calculated energy profiles for both processes represented in Scheme 2 are shown in Fig. 6. The intercepted structures of transition states are reported in the same figure, while the Cartesian coordinates of all the stationary points are reported in Table S6.† As depicted in Fig. 6, the hydrolysis process for the triplet state Tc proceeds in two distinct steps. The initial step of the nucleophilic substitution mechanism involves the rapid entry of a water molecule overcoming a very low activation energy barrier of 1.1 kcal mol^{-1} (TS_{1c}). The water molecule saturates the metal coordination sphere, resulting in the formation of an intermediate with octahedral geometry (T_c–H_2O). In the second step, the mtmp ligand leaves the metal coordination sphere and the pentacoordinated ruthenium complex denoted as the ^{3}Ru–H_2O complex is formed, overcoming an energy barrier of 6.5 kcal mol^{-1} (TS_{2c}). The hydrolysis process for the triplet state Td, instead, takes place in a single step in which a water molecule approaches the pentacoordinated complex, and going through the transition state TS_d, it replaces the mtmp ligand in an associative manner. As anticipated, the formation of the mono-aquated complex occurs, overcoming an energy barrier of 8.4 kcal mol^{-1} (TS_d).

The definitive release of the mtmp ligand and the formation of the Ru–H_2O complex are calculated to be endothermic along both triplet pathways. When a second water molecule comes in close proximity to the ^{3}Ru–H_2O complex, it

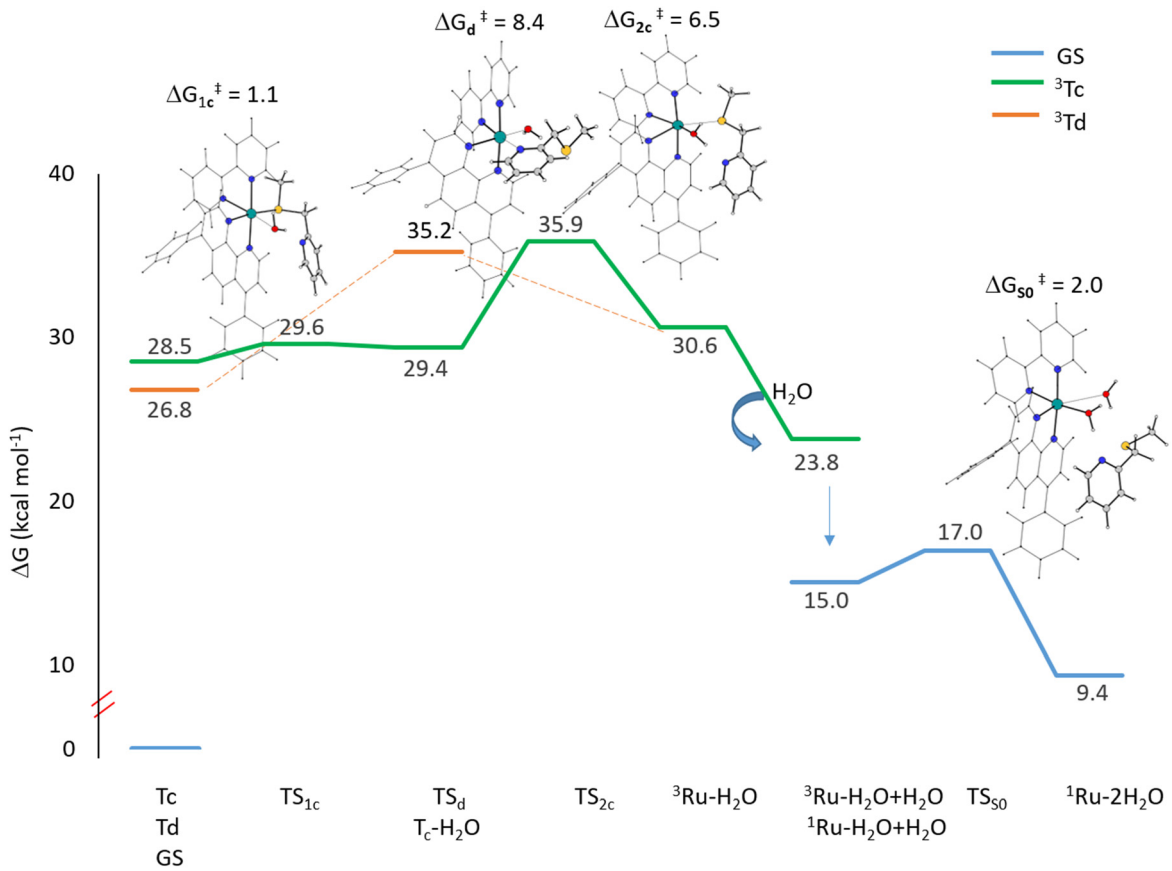

Fig. 6 Calculated free energy profiles in water describing the light-induced substitution mechanism of the **Ru** complex. Relative energies are in kcal mol^{-1} and calculated with respect to the ground state singlet energy of the complex.

Open Access Article. Published on 17 April 2024. Downloaded on 2/20/2026 5:59:16 PM.
This article is licensed under a Creative Commons Attribution-NonCommercial 3.0 Unported Licence.

stabilizes the system by approximately 7 kcal mol^{-1}. Several explorations for the formation of the final biaquated product have been conducted in the triplet state, but all of them failed. This suggests that the formation of the final product, Ru–$2H_2O$, occurs directly in the ground singlet state. Indeed, the solvent adduct of the Ru–H_2O complex in the triplet state undergoes a transition to the corresponding singlet state that lies 15.0 kcal mol^{-1} above the energy of the **Ru** complex. Along the singlet path, a second water molecule binds to the monoaquated Ru complex, overcoming a very low activation energy barrier of only 2.0 kcal mol^{-1}. The final product formation is calculated to be endothermic of 9.4 kcal mol^{-1}. Overall, the results show that for the hydrolysis process to occur, leading to the formation of the cytotoxic agent in PACT, very low energy barriers have to be overcome along calculated pathways, confirming the experimentally detected high efficacy of the studied complex.

Computational details

All molecular geometry optimizations have been carried out with the Gaussian16 software package,[41] at the density functional level of theory, employing the M05 functional.[42] For the **Ru** atom, the relativistic compact Stuttgart–Dresden effective core potential has been used[43] in conjunction with the corresponding split valence basis set. The standard double-ζ 6-31G** basis sets have been used for all the rest of the atoms. The impact of the aqueous solvent has been taken into account by performing optimization of the solvent considering a dielectric constant of 78.4, within the Tomasi implicit polarizable continuum model[44,45] as implemented in Gaussian16. The electronic spectra have been obtained, within the nonequilibrium time-dependent TDDFT approach, as vertical electronic excitation on the ground-state structure, at the same level of theory used for other calculations. Such computational protocol has been selected on the basis of the outcomes of a preliminary benchmark study, considering the performance of several exchange–correlation functionals, on the absorption spectrum of the complex compared with that experimentally detected (Fig. S2 and Table S1†). The optimized structures of all the excited states potentially involved in the complex photoactivation have been explored using the TDDFT approach in a condensed phase. In the case of triplet states, the obtained guesses have then been used as starting points for the optimization within the unrestricted Kohn–Sham formalism.[34,35] Stationary points along the examined reaction pathways have been identified as minima or transition states by the number of imaginary vibrational frequencies (0 or 1, respectively). These calculations have been also used for calculating zero-point energy (ZPE) corrections. Intercepted transition states have been carefully checked to be properly connected to the correct minima by intrinsic reaction coordinate (IRC) analysis.[46,47] To ascertain the probability that a triplet state could be populated, spin–orbit matrix elements have been computed using the quadratic-response TD-DFT approach, as implemented in the ORCA code.[48,49] Relativistic corrections have been obtained by the zeroth order regular approximation (ZORA). ZORA-DEF2-SVP and SARC-ZORA-SVP basis sets have been used for the main and metal atoms, respectively. The RIJCOSX approximations have been introduced to speed up the calculation time, as suggested in the ORCA manual.

Conclusions

Here, a detailed computational investigation of the photophysical properties of a trisheteroleptic ruthenium complex, named the **Ru** complex, having a mtmp ligand that serves as a protecting group towards the coordination of biomolecules present in cells has been carried out by means of DFT and its time-dependent extension. The **Ru** complex is a highly efficacious PACT agent since, upon light irradiation, the "uncaged" complex is released that, as aquated cisplatin, acts as an activated drug able to bind to DNA inducing cell death. All the mechanistic aspects of the photodissociation process have been explored in depth and all the involved states have been fully described. The results of such a detailed investigation provide important information about both the reasons why pyridyl–thioether chelates form excellent caging groups for ruthenium-based PACT compounds and the mechanism by which solvent molecules are involved in the photosubstitution mechanism. First of all, through a comparison of the energies and plots of MOs of **Ru** with those of the other three polypyridyl complexes, it has been demonstrated that the presence of the mtmp ligand causes stabilization of the vacant MOs responsible for the generation of the ^{3}MC states facilitating the population of such dissociative triplet metal-centred states from a triplet with the metal to ligand charge transfer, ^{3}MLCT, character. Once the most appropriate protocol has been chosen, through a benchmark, the experimental spectrum has been reproduced and all the characteristics of singlet and triplet excited states have been explored. Very importantly, calculation of SOC elements for all the triplet states lying below the S1 state shows that they can be populated through efficient ISC. Optimization, using unrestricted DFT, of triplet states identified by TDDFT calculations converged into four distinct triplets denoted as Ta, Tb, Tc and Td, with the former two having the ^{3}MLCT character and the latter two having the ^{3}MC character. Tc and Td triplet states appear to be characterized by a significant reorganization in the coordination sphere of the Ru centre. In particular, Tc shows the detachment of the pyridyl arm of mtmp and Td is characterized, instead, by a clear elongation of the Ru–S bond in comparison with the complex ground state structure. Starting from such triplet states, the mechanism of the mtmp ligand substitution by water leading to the formation of the real cytotoxic species has been elucidated including, for the first time, the role played by the water solvent molecules. The hydrolysis process for the Tc triplet proceeds in two steps consisting of the rapid coordination of a water molecule followed by the mtmp ligand loss due to the definitive detachment of the pyridyl arm. As a result, the pentacoordinated ruthenium complex denoted as ^{3}Ru–H_2O is formed. The same complex is obtained in one step

 This journal is © The Royal Society of Chemistry 2024

Open Access Article. Published on 17 April 2024. Downloaded on 2/20/2026 5:59:16 PM. This article is licensed under a Creative Commons Attribution-NonCommercial 3.0 Unported Licence.

starting from the Td state through an associative substitution reaction causing the definitive breaking of the Ru–S bond. The second water molecule attack leading to the formation of the biaquated Ru–2H_2O complex occurs after the transition to the corresponding singlet state, overcoming a very low energy barrier. The outcomes of our computational analysis confirm that electronic effects can play a very important role in promoting photosubstitution, as it happens in the present case, due to the ^{3}MC state stabilization.

Author contributions

The manuscript was written through contributions of all authors. All authors have given approval to the final version of the manuscript.

Conflicts of interest

There are no conflicts to declare.

Acknowledgements

This research was supported by the Italian Association for Cancer Research, AIRC (ID 25578). The authors gratefully acknowledge the computing time granted by the CINECA (project IsCa3_MoAPACT).

References

1 X. Wang, X. Wang, S. Jin, N. Muhammad and Z. Guo, Stimuli-Responsive Therapeutic Metallodrugs, *Chem. Rev.*, 2019, **119**, 1138–1192.
2 N. J. Farrer, L. Salassa and P. J. Sadler, Photoactivated chemotherapy (PACT): the potential of excited-state d-block metals in medicine, *Dalton Trans.*, 2009, 10690–10701.
3 U. Schatzschneider, Photoactivated Biological Activity of Transition-Metal Complexes, *Eur. J. Inorg. Chem.*, 2010, 1451–1467.
4 L. Galluzzi, L. Senovilla, I. Vitale, J. Michels, I. Martins, O. Kepp, M. Castedo and G. Kroemer, Molecular mechanisms of cisplatin resistance, *Oncogene*, 2012, **31**, 1869–1883.
5 E. Wexselblatt, E. Yavin and D. Gibson, Cellular interactions of platinum drugs, *Inorg. Chim. Acta*, 2012, **393**, 75–83.
6 S. Bonnet, Why develop photoactivated chemotherapy?, *Dalton Trans.*, 2018, **47**, 10330–10343.
7 N. J. Farrer, J. A. Woods, L. Salassa, Y. Zhao, K. S. Robinson, G. Clarkson, F. S. Mackay and P. J. Sadler, A Potent Trans-Diimine Platinum Anticancer Complex Photoactivated by Visible Light, *Angew. Chem., Int. Ed.*, 2010, **49**, 8905–8908.
8 I. Chakraborty, J. Jimenez and P. K. Mascharak, CO-Induced apoptotic death of colorectal cancer cells by a luminescent photoCORM grafted on biocompatible carboxymethyl chitosan, *Chem. Commun.*, 2017, **53**, 5519–5522.
9 A. Kastl, A. Wilbuer, A. L. Merkel, L. Feng, P. D. Fazio, M. Ocker and E. Meggers, Dual anticancer activity in a single compound: visible-light-induced apoptosis by an antiangiogenic iridium complex, *Chem. Commun.*, 2012, **48**, 1863–1865.
10 M. R. Kim, H. Morrison and S. I. Mohammed, Effect of a photoactivated rhodium complex in melanoma, *Anticancer Drugs*, 2011, **22**, 896–904.
11 Z. Li, A. David, B. A. Albani, J.-P. Pellois, C. Turro and K. R. Dunbar, Optimizing the Electronic Properties of Photoactive Anticancer Oxypyridine-Bridged Dirhodium(II, II) Complexes, *J. Am. Chem. Soc.*, 2014, **136**, 17058–17070.
12 D. A. Lutterman, P. K.-L. Fu and C. Turro, cis-[Rh2(μ-O2CCH$_3$)2(CH$_3$CN)6]2+ as a Photoactivated Cisplatin Analog, *J. Am. Chem. Soc.*, 2006, **128**, 738–739.
13 L. Zhang, P. Wang, X.-Q. Zhou, L. Bretin, X. Zeng, Y. Husiev, E. A. Polanco, G. Zhao, L. S. Wijaya, T. Biver, S. E. Le Dévédec, W. Sun and S. Bonnet, Cyclic Ruthenium-Peptide Conjugates as Integrin-Targeting Phototherapeutic Prodrugs for the Treatment of Brain Tumors, *J. Am. Chem. Soc.*, 2023, **145**, 14963–14980.
14 D. Havrylyuk, D. K. Heidary, Y. Sun, S. Parkin and E. C. Glazer, Photochemical and Photobiological Properties of Pyridyl-pyrazol(in)e-Based Ruthenium(II) Complexes with Sub-micromolar Cytotoxicity for Phototherapy, *ACS Omega*, 2020, **5**, 18894–18906.
15 S. Bonnet, Ruthenium-Based Photoactivated Chemotherapy, *J. Am. Chem. Soc.*, 2023, **145**, 23397–23415.
16 L. Conti, E. Macedi, C. Giorgi, B. Valtancoli and V. Fusi, Combination of light and Ru(II) polypyridyl complexes: Recent advances in the development of new anticancer drugs, *Coord. Chem. Rev.*, 2022, **469**, 214656.
17 T. N. Singh and C. Turro, Photoinitiated DNA Binding by cis-[Ru(bpy)2(NH3)2]2+, *Inorg. Chem.*, 2004, **43**, 7260–7262.
18 Q. Chen, J.-A. Cuello-Garibo, L. Bretin, L. Zhang, V. Ramu, Y. Aydar, Y. Batsiun, S. Bronkhorst, Y. Husiev, N. Beztsinna, L. Chen, X.-Q. Zhou, C. Schmidt, I. Ott, M. J. Jager, A. M. Brouwer, B. E. Snaar-Jagalska and S. Bonnet, Photosubstitution in a trisheteroleptic ruthenium complex inhibits conjunctival melanoma growth in a zebrafish orthotopic xenograft model, *Chem. Sci.*, 2022, **13**, 6899–6919.
19 R. N. Garner, L. E. Joyce and C. Turro, Effect of Electronic Structure on the Photoinduced Ligand Exchange of Ru(II) Polypyridine Complexes, *Inorg. Chem.*, 2011, **50**, 4384–4391.
20 J. D. Knoll, B. A. Albani and C. Turro, New Ru(II) Complexes for Dual Photoreactivity: Ligand Exchange and 1O2 Generation, *Acc. Chem. Res.*, 2015, **48**, 2280–2287.
21 C. Kreitner and K. Heinze, Excited state decay of cyclometalated polypyridine ruthenium complexes: insight from theory and experiment, *Dalton Trans.*, 2016, **45**, 13631–13647.

Open Access Article. Published on 17 April 2024. Downloaded on 2/20/2026 5:59:16 PM. This article is licensed under a Creative Commons Attribution-NonCommercial 3.0 Unported Licence.

22 M. Kayanuma, Photosubstitution reaction of a bidentate ligand in a Ru(II) complex in aqueous solution, *Comput. Theor. Chem.*, 2022, **1213**, 113745.
23 A. Soupart, F. Alary, J.-L. Heully, P. I. P. Elliott and I. M. Dixon, Theoretical Study of the Full Photosolvolysis Mechanism of [Ru(bpy)3]2+: Providing a General Mechanistic Roadmap for the Photochemistry of [Ru(N^N)3]2+-Type Complexes toward Both Cis and Trans Photoproducts, *Inorg. Chem.*, 2020, **59**, 14679–14695.
24 M. L. A. Hakkennes, M. S. Meijer, J. P. Menzel, A.-C. Goetz, R. Van Duijn, M. A. Siegler, F. Buda and S. Bonnet, Ligand Rigidity Steers the Selectivity and Efficiency of the Photosubstitution Reaction of Strained Ruthenium Polypyridyl Complexes, *J. Am. Chem. Soc.*, 2023, **145**, 13420–13434.
25 R. L. Martin, Natural transition orbitals, *J. Chem. Phys.*, 2003, **118**, 4775–4777.
26 F. Plasser, TheoDORE: A toolbox for a detailed and automated analysis of electronic excited state computations, *J. Chem. Phys.*, 2020, **152**, 084108.
27 J. S. García, F. Alary, M. Boggio-Pasqua, I. M. Dixon and J.-L. Heully, Is photoisomerization required for NO photorelease in ruthenium nitrosyl complexes?, *J. Mol. Model*, 2016, **22**, 284.
28 S. E. Greenough, G. M. Roberts, N. A. Smith, M. D. Horbury, R. G. McKinlay, J. M. Żurek, M. J. Paterson, P. J. Sadler and V. G. Stavros, Ultrafast photo-induced ligand solvolysis of cis-[Ru(bipyridine)2(nicotinamide)2]2+: experimental and theoretical insight into its photoactivation mechanism, *Phys. Chem. Chem. Phys.*, 2014, **16**, 19141–19155.
29 J. D. Knoll, B. A. Albani and C. Turro, New Ru(II) Complexes for Dual Photoreactivity: Ligand Exchange and 1O2 Generation, *Acc. Chem. Res.*, 2015, **48**, 2280–2287.
30 C.-W. Yin, M.-K. Tsai and Y. J. Chen, Low-Temperature Observation of the Excited-State Decay of Ruthenium-(Mono-2,2′:6′,2″-Terpyridine) Ions with Innocent Ligands: DFT Modeling of an 3MLCT–3MC Intersystem Crossing Pathway, *ACS Omega*, 2023, **8**, 11623–11633.
31 M. Kasha, Characterization of electronic transitions in complex molecules, *Discuss. Faraday Soc.*, 1950, **9**, 14–19.
32 F. Ponte, D. M. Scopelliti, N. Sanna, E. Sicilia and G. Mazzone, How Computations Can Assist the Rational Design of Drugs for Photodynamic Therapy: Photosensitizing Activity Assessment of a Ru(II)-BODIPY Assembly, *Molecules*, 2022, **27**, 5635.
33 F. Ponte, S. Scoditti, P. Barretta and G. Mazzone, Computational Assessment of a Dual-Action Ru(II)-Based Complex: Photosensitizer in Photodynamic Therapy and Intercalating Agent for Inducing DNA Damage, *Inorg. Chem.*, 2023, **62**, 8948–8959.
34 D. Escudero, E. Heuser, R. J. Meier, M. Schäferling, W. Thiel and E. Holder, Unveiling Photodeactivation Pathways for a New Iridium(III) Cyclometalated Complex, *Chem. – Eur. J.*, 2013, **19**, 15639–15644.
35 D. Escudero, W. Thiel and B. Champagne, Spectroscopic and second-order nonlinear optical properties of Ruthenium(II) complexes: a DFT/MRCI and ADC(2) study, *Phys. Chem. Chem. Phys.*, 2015, **17**, 18908–18912.
36 Y.-J. Tu, S. Mazumder, J. F. Endicott, C. Turro, J. J. Kodanko and H. B. Schlegel, Selective Photodissociation of Acetonitrile Ligands in Ruthenium Polypyridyl Complexes Studied by Density Functional Theory, *Inorg. Chem.*, 2015, **54**, 8003–8011.
37 E. Wachter, D. K. Heidary, B. S. Howerton, S. Parkin and E. C. Glazer, Light-activated ruthenium complexes photobind DNA and are cytotoxic in the photodynamic therapy window, *Chem. Commun.*, 2012, **48**, 9649–9651.
38 B. S. Howerton, D. K. Heidary and E. C. Glazer, Strained Ruthenium Complexes Are Potent Light-Activated Anticancer Agents, *J. Am. Chem. Soc.*, 2012, **134**, 8324–8327.
39 J. Roque III, D. Havrylyuk, P. C. Barrett, T. Sainuddin, J. McCain, K. Colón, W. T. Sparks, E. Bradner, S. Monro, D. Heidary, C. G. Cameron, E. C. Glazer and S. A. McFarland, Strained, Photoejecting Ru(II) Complexes that are Cytotoxic Under Hypoxic Conditions, *Photochem. Photobiol.*, 2020, **96**, 327–339.
40 C. E. Welby, G. K. Armitage, H. Bartley, A. Sinopoli, B. S. Uppal and P. I. P. Elliott, Photochemical ligand ejection from non-sterically promoted Ru(ii)bis(diimine) 4,4′-bi-1,2,3-triazolyl complexes, *Photochem. Photobiol. Sci.*, 2014, **13**, 735–738.
41 M. J. Frisch, G. W. Trucks, H. B. Schlegel, G. E. Scuseria, M. A. Robb, J. R. Cheeseman, G. Scalmani, V. Barone, G. A. Petersson, H. Nakatsuji, X. Li, M. Caricato, A. V. Marenich, J. Bloino, B. G. Janesko, R. Gomperts, B. Mennucci, H. P. Hratchian, J. V. Ortiz, A. F. Izmaylov, J. L. Sonnenberg, D. Williams-Young, F. Ding, F. Lipparini, F. Egidi, J. Goings, B. Peng, A. Petrone, T. Henderson, D. Ranasinghe, V. G. Zakrzewski, J. Gao, N. Rega, G. Zheng, W. Liang, M. Hada, M. Ehara, K. Toyota, R. Fukuda, J. Hasegawa, M. Ishida, T. Nakajima, Y. Honda, O. Kitao, H. Nakai, T. Vreven, K. Throssell, J. A. Montgomery Jr, J. E. Peralta, F. Ogliaro, M. J. Bearpark, J. J. Heyd, E. N. Brothers, K. N. Kudin, V. N. Staroverov, T. A. Keith, R. Kobayashi, J. Normand, K. Raghavachari, A. P. Rendell, J. C. Burant, S. S. Iyengar, J. Tomasi, M. Cossi, J. M. Millam, M. Klene, C. Adamo, R. Cammi, J. W. Ochterski, R. L. Martin, K. Morokuma, O. Farkas, J. B. Foresman and D. J. Fox, *Gaussian 16, Revision B.01*, Gaussian, Inc., Wallingford CT, 2016. GaussView 5.0. Wallingford, E.U.A.
42 Y. Zhao, N. E. Schultz and D. G. Truhlar, Exchange-correlation functional with broad accuracy for metallic and nonmetallic compounds, kinetics, and noncovalent interactions, *J. Chem. Phys.*, 2005, **123**, 161103.
43 D. Andrae, U. Häußermann, M. Dolg, H. Stoll and H. Preuß, Energy-adjusted ab initio pseudopotentials for the second and third row transition elements, *Theor. Chim. Acta*, 1990, **77**, 123–141.
44 S. Miertuš, E. Scrocco and J. Tomasi, Electrostatic interaction of a solute with a continuum. A direct utilizaion of

 This journal is © The Royal Society of Chemistry 2024

Open Access Article. Published on 17 April 2024. Downloaded on 2/20/2026 5:59:16 PM.
This article is licensed under a Creative Commons Attribution-NonCommercial 3.0 Unported Licence.

AB initio molecular potentials for the prevision of solvent effects, *Chem. Phys.*, 1981, **55**, 117–129.

45 S. Miertuš and J. Tomasi, Approximate evaluations of the electrostatic free energy and internal energy changes in solution processes, *Chem. Phys.*, 1982, **65**, 239–245.

46 K. Fukui, Formulation of the reaction coordinate, *J. Phys. Chem.*, 1970, **74**, 4161–4163.

47 C. Gonzalez and H. B. Schlegel, An improved algorithm for reaction path following, *J. Chem. Phys.*, 1989, **90**, 2154–2161.

48 F. Neese, The ORCA program system, *Wiley Interdiscip. Rev. Comput. Mol. Sci.*, 2012, **2**, 73–78.

49 F. Neese, Software update: the ORCA program system, version 4.0, *Wiley Interdiscip. Rev. Comput. Mol. Sci.*, 2018, **8**, e1327.